Journal of Materials Chemistry A

RSC Publishing

PAPER

View Article Online
View Journal | View Issue

Cite this: J. Mater. Chem. A, 2013, 1, 4516

C/B codoping effect on band gap narrowing and optical performance of TiO_2 photocatalyst: a spin-polarized DFT study

Yanming Lin,[ab] Zhenyi Jiang,*[a] Chaoyuan Zhu,[b] Xiaoyun Hu,[c] Xiaodong Zhang,[a] Haiyan Zhu,[a] Jun Fan[d] and Sheng Hsien Lin[be]

Received 29th November 2012
Accepted 31st January 2013

DOI: 10.1039/c3ta01298k

www.rsc.org/MaterialsA

The electronic and optical properties of several possible C/B-codoped models of anatase and rutile TiO_2 have been investigated systematically using spin-polarized density functional theory calculations. Our calculated results show that the synergistic effect of C/B codoping can induce some hybridized energy states appearing in the forbidden gap and the band gap has a narrowing in anatase and rutile TiO_2, which can lead to a decrease of the photon excitation energy and an obvious red-shift of the optical absorption edge. These results lead to an excellent photocatalytic activity in C/B-codoped TiO_2. Moreover, with the increase of C and B impurities' concentration in anatase and rutile TiO_2, we find that the intensity of impurity states has a strengthening in the band gap, the position of impurity states changes, and the visible-light absorption performance improves gradually.

1 Introduction

Titanium dioxide (TiO_2) has attracted great attention as a promising metal oxide for applications in photocatalysts, water splitting for hydrogen production, and solar cells due to its excellent physical and chemical properties, such as high oxidative power, long term stability, non-toxicity, and low cost.[1–6] However, its universal use is restricted to ultraviolet-light (λ < 390 nm) due to the wide band gap of TiO_2 (3.2 eV for anatase structure[7] and 3.0 eV for rutile structure[8]). Furthermore, photoexcited electron–hole pairs tend to recombine relatively easily in TiO_2.[9] Both of these factors limit possible applications in photocatalytic materials' design. Therefore, reducing the band gap of TiO_2 to make it photosensitive to the visible-light region with low electron–hole recombination has become one of the most important goals in photocatalyst studies.

To extend the optical absorption of TiO_2-based materials to the visible-light region and to obtain the maximum amount of energy from the solar spectrum, doping TiO_2 with non-metal elements has been used widely. For instance, Jin *et al.*[10] reported that the photocatalytic activity of Si-doped TiO_2 prepared *via* hydrothermal process is higher than that of Degussa P25 and pure TiO_2. Yang *et al.* studied the geometrical structures and electronic properties of Si-doped TiO_2.[11] The results show that substitutional Si-doping leads to a band gap narrowing in TiO_2, which may be responsible for the experimental red-shift of the optical absorption edge. Asahi *et al.* showed that substituting O with N was an effective approach to achieve a band gap narrowing.[12] Then, a large number of experimental and theoretical studies also indicated that localized N 2p states located close to the valence band maximum led to the absorption of visible-light.[13–18] Umebayashi *et al.* have reported that S-doping into the lattice of TiO_2 will lead to band gap narrowing, and later theoretical studies showed that impurity states of S 3p on the upper edge of the valence band induce a red-shift of the optical absorption edge.[19–22]

In addition, C-doped TiO_2 has been synthesized and corresponding theories have also been reported.[5,23–25] For example, the study of Valentin *et al.*[23] indicates that carbon impurities result in modest variations of the band gap and induce several localized occupied states in the band gap, which may account for the experimentally observed red-shift of the optical absorption edge towards the visible-light region. And their results also indicate that carbon doping may favor the formation of oxygen vacancies in bulk TiO_2. The photocatalytic activity of B-doped TiO_2 has been widely investigated.[26–30] Zhao *et al.* reported that B-doped TiO_2 showed a substantial red-shift of the optical absorption edge and the photocatalytic activity was greatly enhanced as it was further loaded with Ni_2O_3.[26] Some research indicates that codoping of different non-metal elements into TiO_2 can further narrow its band gap and improve its photocatalytic activity. For example, Jia *et al.* studied the microscopic mechanism for band gap narrowing and the origin

[a]Institute of Modern Physics, Northwest University, Xi'an 710069, P. R. China. E-mail: jiangzy@nwu.edu.cn; linymnwu@gmail.com; Fax: +86-29-88302331; Tel: +86-29-88303491

[b]Department of Applied Chemistry, Institute of Molecular Science and Center for Interdisciplinary Molecular Science, National Chiao-Tung University, Hsinchu 30050, Taiwan

[c]Department of Physics, Northwest University, Xi'an 710069, P. R. China

[d]School of Chemical Engineering, Northwest University, Xi'an 710069, P. R. China

[e]Institute of Atomic and Molecular Sciences, Academia Sinica, Taipei 106, Taiwan

of the enhanced visible-light photocatalytic activity in N/S-codoped anatase TiO_2.[31] Li *et al.* reported that C/H-codoping produces significant band gap narrowing, which leads to higher visible-light photocatalytic efficiency than C-doped anatase TiO_2.[32] Long and English investigated systematically the influence on electronic properties of anatase TiO_2 codoping by N and Si using Heyd–Scuseria–Ernzerhof (HSE06) hybrid density functional theory calculations.[33] These results indicate that non-metal codoping is one of the most effective approaches to extend the absorption edge of TiO_2 to the visible-light range.

Recently, Wu *et al.* prepared firstly a C/B-codoped TiO_2 photocatalyst by the gel–hydrothermal method.[34] The experimental results show that the C/B-codoped TiO_2 samples exhibit a stronger optical adsorption and higher photocatalytic activity in the visible-light region than pure TiO_2. However, to the best of our knowledge, there have been few reports regarding the physical and chemical origin of photocatalytic activity of C/B-codoped TiO_2 and some basic questions about the character of C and B impurities, such as C, B doping effect on the geometry and electronic structures *etc.* To address these questions, in the present work, we investigated the electronic and optical properties of several possible C/B-codoped models of anatase and rutile TiO_2 systematically using spin-polarized density functional theory (DFT) calculations. The theoretical analysis provided a possible explanation for the experimentally observed red-shift of optical absorption edge and outstanding photocatalytic activity in C/B-codoped TiO_2.

2 Computation model and methods

All the spin-polarized DFT calculations were performed using the projector augmented wave pseudopotentials as implemented in the VASP code.[35,36] The exchange correlation function was treated by the generalized gradient approximation (GGA) with the Perdew–Wang parameterization (known as GGA-PW91).[37] The Brillouin-zone integrations were approximated by using the special *k*-point sampling of the Monhkorst–Pack scheme.[38] A cutoff energy of 500 eV and a mesh size of $5 \times 5 \times 5$ were used for geometry optimization and electronic property calculations. Using the block Davidson scheme, both the atomic positions and cell parameters were optimized until the residual forces were below 0.01 eV $Å^{-1}$. It is well-known that the traditional DFT method usually underestimates the band gap for semiconductors. However, the DFT + U approach introduces an on-site correction in order to describe systems with localized d electrons, which can produce a better band gap in comparison with experimental results. Therefore, all our calculations of the electronic and optical properties were conducted using the GGA + U method[39–42] for Ti 3d electrons. It was found that the band gap of pure TiO_2 was 2.90 eV for anatase structure and 2.67 eV for rutile structure with $U = 10.0$ eV and $J = 1.0$ eV for Ti 3d electrons, and was only weakly dependent on the J value.

The valence electron configurations considered in this study included Ti ($3d^2 4s^2$), O ($2s^2 2p^4$), C ($2s^2 2p^2$), and B ($2s^2 2p^1$). All the doping systems were constructed from a relaxed ($2 \times 2 \times 1$) 48-atom anatase and a relaxed ($2 \times 2 \times 2$) 48-atom rutile TiO_2 supercells, as are shown in Fig. 1. A variety of possible C or/and B (co)doped anatase and rutile TiO_2 structures were considered by replacing an oxygen or titanium atom in the lattice with a carbon or boron atom, such as substitutional C at the Ti site (C@Ti), substitutional C at the O site (C@O), substitutional B at the Ti site (B@Ti), and substitutional B at the O site (B@O) for the bulk monodoped systems. For codoped systems, C locates either at Ti or at O and B locates either at O or at Ti, such as C@Ti&B@Ti, C@O&B@O, C@Ti&B@O, and C@O&B@Ti. The partial geometries taken from the structures optimized for C or/and B (co)doped anatase and rutile TiO_2 supercells are shown in Fig. 2 and 3.

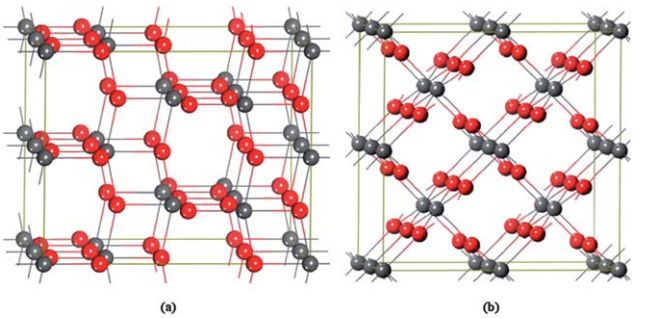

Fig. 1 (a) Anatase supercell ($Ti_{16}O_{32}$) and (b) rutile supercell ($Ti_{16}O_{32}$). The gray spheres represent Ti atoms, and the red spheres represent O atoms.

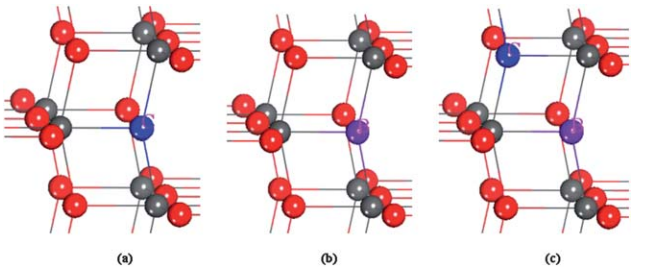

Fig. 2 Optimized partial structures using the 48-atom $2 \times 2 \times 1$ anatase TiO_2 supercell: (a) C-doped (C@O), (b) B-doped (B@O), and (c) C/B-codoped (C@O&B@O). The gray spheres and red spheres represent the Ti and O atoms, respectively. The blue spheres and purple spheres represent C and B atoms, respectively.

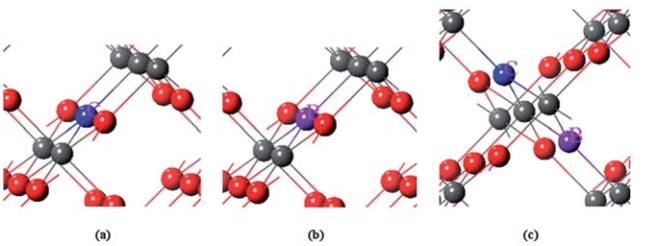

Fig. 3 Optimized partial structures using the 48-atom $2 \times 2 \times 2$ rutile TiO_2 supercell: (a) C-doped (C@O), (b) B-doped (B@O), and (c) C/B-codoped (C@O&B@O). The gray spheres and red spheres represent the Ti and O atoms, respectively. The blue spheres and purples sphere represent C and B atoms, respectively.

3 Results and discussion

Model structures of C or/and B doped anatase and rutile TiO_2

In our calculations, we considered two possible monodoping ways to introduce C or B atoms into the anatase and rutile lattices of TiO_2. The first one is an O atom replaced with a C or B atom (C@O or B@O); the second one is a Ti atom replaced with a C or B atom (C@Ti or B@Ti). For codoped models, we considered similarly four possible ways to introduce C/B atoms into the anatase and rutile lattices of TiO_2. The first one is two O atoms replaced with a C and B atom (C@O&B@O); the second one is two Ti atoms replaced with a C and B atom (C@Ti&B@Ti); the third one is a Ti and an O atom replaced with a C and B atom, respectively (C@Ti&B@O); the last one is an O and a Ti atom replaced with a C and B atom, respectively (C@O&B@Ti).

We optimized geometry structures of the doped anatase and rutile TiO_2 supercells (48 atoms) by the DFT calculations; the optimized lattice parameters, volumes, and impurity atomic coordinates are shown in Table 1. For the anatase phase of TiO_2, our calculated lattice parameters are $a = b = 3.774$ Å, $c = 9.409$ Å, which are consistent with the experimental values.[43] The data of Table 1 show that the lattice constants have a tiny change in the different models, and the volume of the unit cell increases with the impurity atom(s) of C or/and B doping. This can be understood by the fact that the radii of impurity atoms C (0.91 Å) and B (1.17 Å) are larger than that of O (0.65 Å). The optimised coordinates of the impurity atoms (C or/and B) are listed in Table 1. The partial geometries taken from the optimized C or/and B doped anatase TiO_2 supercell are shown in Fig. 2. The average bond lengths of the doped anatase TiO_2 after geometry optimization are summarized in Table 2. For pure anatase TiO_2, the average Ti–O bond length is 1.981 Å, there is no significant change compared with those of the C- and B-doped structures. The average Ti–O bond length of the C/B-codoped TiO_2 in the supercell is shorter than C- and B-doped TiO_2. The Ti–C bond length in C-doped and C/B-codoped systems are longer than the Ti–O bond length as the radius of the C atom is larger than that of the O atom. Due to the larger radius of B, the Ti–B bond length of B-doped and C/B-codoped TiO_2 is also longer than that of the Ti–O bond. In the case of codoped TiO_2, the length of all these bonds have an increase, and the Ti–B bond length is 2.136 Å.

Table 2 Average bond lengths of doped anatase TiO_2 after geometry optimization (in Å)

Bond length (Å)	Pure anatase	C-doped	B-doped	C/B-codoped
Ti–O	1.981	2.056	2.108	1.984
Ti–C	—	2.156	—	2.004
Ti–B	—	—	2.291	2.022
C–B	—	—	—	2.136

For the rutile phase of TiO_2, the calculated parameters of the unit cell are $a = b = 4.566$ Å, $c = 2.950$ Å, which agree with the experimental data.[43] The data of Table 1 show that the lattice parameters have a tiny change in the different models, and the volume of the unit cell increases with the impurity atom(s) of C or/and B doping. The optimised coordinates for the impurity atoms (C or/and B) of the model are obtained by DFT calculations, and are shown in Table 1. Fig. 3 gives the partial geometries taken from the structure optimized C or/and B doped rutile TiO_2 supercell. The average bond lengths of the doped rutile TiO_2 after geometry optimization are listed in Table 3. For pure rutile TiO_2, the average Ti–O bond length is 1.958 Å, showing no significant change compared with those of the C- and B-doped structures. However, the average Ti–O bond length of the C/B-codoped TiO_2 in the supercell is longer than C- and B-doped TiO_2. The Ti–C bond lengths in C-doped and C/B-codoped systems are longer than the Ti–O bond length as the radius of the C atom is larger than that of the O atom. Due to the larger radius of B, the Ti–B bond lengths of B-doped and C/B-codoped TiO_2 are also longer than that of the Ti–O bond. For C/B-codoped TiO_2, the Ti–B bond length is 1.973 Å, and the lengths of the other bonds have increased, too.

These calculated results indicate that C/B codoping can lead to a significant lattice deformation and a high defect formation energy in anatase and rutile TiO_2, which in turn changes the dipole moments and makes the separation of photoexcited electron–hole pairs easier.

Table 1 The volume change of the doped 48-atom anatase and rutile TiO_2 supercells. The cell volume is in $Å^3$ for one TiO_2 formula unit

Phase	Space group	Doping model	Lattice parameters (Å)			Volume/f.u. ($Å^3$)	Impurity atomic coordinates
			a	*b*	*c*		
Anatase	$I4_1/amd$ (141 #) tetragonal	Pure (expt.[a])	3.782	3.782	9.502	34.070	—
		Pure (calc.)	3.774	3.774	9.409	33.498	
		C-doped (C@O)	3.797	3.780	9.457	33.936	C (0.5000, 0.2500, 0.4756)
		B-doped (B@O)	3.817	3.771	9.461	34.046	B (0.5000, 0.2500, 0.4926)
		C/B-codoped (C@O&B@O)	3.775	3.773	9.603	34.191	C (0.2992, 0.2500, 0.3296) B (0.4460, 0.2500, 0.4246)
Rutile	$P4_2/mnm$ (136 #) tetragonal	Pure (expt.[a])	4.593	4.593	2.959	31.210	—
		Pure (calc.)	4.566	4.566	2.950	30.751	
		C-doped (C@O)	4.578	4.578	2.951	30.923	C (0.3538, 0.3538, 0.5000)
		B-doped (B@O)	4.591	4.591	2.952	31.106	B (0.3556, 0.3556, 0.5000)
		C/B-codoped (C@O&B@O)	4.548	4.548	3.019	31.214	C (0.4606, 0.5394, 0.7500), B (0.5751, 0.4249, 0.7500)

[a] Ref. 44.

Table 3 Average bond lengths of the doped rutile TiO_2 after geometry optimization (in Å)

Bond length (Å)	Pure rutile	C-doped	B-doped	C/B-codoped
Ti–O	1.958	1.919	1.880	1.964
Ti–C	—	2.023	—	2.009
Ti–B	—	—	2.097	2.132
C–B	—	—	—	1.973

Defect formation energy

To probe the stabilities of the doped systems, we calculated the defect formation energies (E_f) for the monodoped and codoped systems according to the formulae

$$E_{f(X@Y)} = E_{(X@Y)} - E_{(pure)} - (\mu_X - \mu_Y) \quad (1)$$

$$E_{f(C@Y\&B@Y)} = E_{(C@Y\&B@Y)} - E_{(pure)} - (\mu_C + \mu_B - \mu_Y - \mu_Y) \quad (2)$$

$$(X = C, B;\ Y = Ti, O)$$

where $E_{(pure)}$ is the total energy of the host pure TiO_2 supercell, $E_{(X@Y)}$ and $E_{(C@Y\&B@Y)}$ are total energies of the monodoped and codoped systems, respectively. Under equilibrium conditions, the concentration of a point defect is controlled by its formation energy, which depends on the chemical potentials of the host and impurity atoms. For TiO_2, the chemical potentials of O and Ti satisfy the relationship $\mu_{Ti} + 2\mu_O = \mu_{TiO_2}$, $\mu_O \leq \mu_{O_2}/2$, and $\mu_{Ti} \leq \mu_{Ti_{metal}}$. The chemical potential μ_O is determined by the energy of an O_2 molecule in the O-rich growth condition (corresponding to a high value of μ_O). By referencing μ_O to the energy of an O atom in the O_2 molecule, μ_{Ti} in the Ti-rich condition (corresponding to a high value of μ_{Ti}) amounts to the energy of one Ti atom in bulk Ti. μ_C is the chemical potential of C impurity, which is calculated from bulk C. μ_B is the chemical potential of B impurity, which is calculated by the bulk BN and N_2 molecules ($\mu_B = \mu_{BN} - \mu_N$, $\mu_N = \mu_{N_2}/2$).

Our calculations for a variety of possible doping models gave a successful explanation, and the ion of dopant may be dependent on the growth condition. It should be noted that the smaller the E_f value is, the easier it is to incorporate impurity ions into the TiO_2 supercell. Our calculated formation energies for all of (co)doped anatase and rutile TiO_2 are listed in Table 4. It can be observed that the formation energy of C@O is much smaller than that of C@Ti under both Ti-rich and O-rich growth conditions in C-doped anatase and rutile TiO_2, suggesting that the O atom is easier to be replaced with the C atom under both Ti-rich and O-rich growth conditions. In particular, under the O-rich growth condition, the formation energy of C@O is negative in the anatase TiO_2 supercell, indicating that the C impurity is readily incorporated into the crystal of anatase TiO_2; partial geometries are shown in Fig. 2(a) and 3(a). For B-doped anatase and rutile TiO_2, our calculations suggest that the formation energy of B@O is still lower than that of B@Ti under both Ti-rich and O-rich growth conditions, indicating that the O atom is easier to be replaced with the B atom under both Ti-rich and O-rich growth conditions; partial geometries are shown in Fig. 2(b) and 3(b). For C locating either at Ti or at O and B locating either at O or at Ti in codoped systems, the formation energies of C@O&B@O codoped model is much smaller than those of the other codoped systems under both Ti-rich and O-rich growth conditions. In particular, under the O-rich growth condition, the formation energy of C@O&B@O is negative in anatase TiO_2 supercell, indicating that the C and B impurities are readily incorporated into the crystal of anatase TiO_2. These results indicate that C and B impurities are preferred to substitute the O ion under both Ti-rich and O-rich growth conditions, Fig. 2(c) and 3(c) show the corresponding partial geometries. Moreover, in order to study the distance dependence between the C/B codopants, we have calculated the defect formation energy and band gap of C/B-codoped TiO_2 using the 216-atom ($3 \times 3 \times 2$) anatase and 162-atom ($3 \times 3 \times 3$) rutile TiO_2 supercells. The calculated results indicate that the defect formation energy increases gradually with the increase of the distance between the C/B codopants, but with almost no change of the band gap.

Table 4 Defect formation energies of doped anatase and rutile TiO_2 systems (in eV)

		Defect formation energy (eV)			
		Anatase		Rutile	
Doped systems		Ti-rich	O-rich	Ti-rich	O-rich
Doped	C@Ti	12.2422	10.3195	13.5925	11.6698
	C@O	3.5698	−0.3035	4.3246	1.0222
	B@Ti	10.9707	9.0480	11.7642	9.8415
	B@O	7.2360	3.9336	7.9429	4.6405
Codoped	C@Ti&B@Ti	18.4859	14.6405	21.3417	17.4963
	C@O&B@O	6.1546	−0.4502	10.0967	3.4919
	C@Ti&B@O	14.7445	9.5194	14.5516	9.3265
	C@O&B@Ti	12.1427	6.9176	12.7302	7.5051

Electronic structures

To understand the effects of C or/and B doping on the photocatalytic activity and optical absorption properties of anatase and rutile TiO_2, the electronic structures of all the (co)doped models are calculated. As the traditional DFT method seriously underestimates the band gap for semiconductors,[44–46] we calculated the electronic structure using the DFT + U method, and the calculated band gaps are 2.90 eV and 2.67 eV for anatase and rutile TiO_2, respectively. These calculated results are consistent with the experimental value of 3.20 eV for anatase structure[47] and 3.00 eV for rutile structure.[8,48,49]

The total density of states (TDOS) and partial density of states (PDOS) of the (co)doped anatase TiO_2 are calculated and plotted in Fig. 4 for all the pure and doped anatase TiO_2 models, with up-spin DOS above zero and down-spin DOS below zero. For comparison, the TDOS and PDOS of pure anatase that were calculated (see Fig. 4(a) and (a′)) indicate that the valence band (VB) mainly consists of O 2p states with a large bandwidth,

showing strong delocalization and bonding characteristic among the O 2p electrons, while the conduction band (CB) is mainly contributed to by the Ti 3d states. For C-doped anatase TiO_2 (C@O) (see Fig. 4(b) and (b′)), a series of impurity energy levels (C 2p orbital) appear in the forbidden gap, and all of the impurity energy levels are located above the valence band maximum (VBM) and below the conduction band minimum (CBM). Therefore, the band gap should be much smaller than the pure anatase TiO_2 if measured from the occupied states above the VBM to CBM, which can possibly explain why C-doped TiO_2 has better visible-light photocatalytic activity and shows the red-shift phenomenon of the optical absorption edge compared to pure TiO_2 reported in the experiment.[34] For B-doped anatase TiO_2 (B@O) (see Fig. 4(c) and (c′)), the calculated TDOS shows that the top of the VB has a little shift and the conduction bandwidth has a little increase compared with the pure anatase TiO_2. Moreover, some gap states are located in the forbidden gap and mix with the CB edge, and further PDOS calculations based on the Mulliken population analysis[50,51] show that the gap states mostly consist of the B 2p orbital and adjacent Ti 3d and O 2p orbitals. Hence, the electron excitations from the VB to the unoccupied gap states above the VBM may induce a red-shift of the optical absorption edge, which is consistent with experimental measurements that the incorporation of B atoms in anatase TiO_2 results in a red-shift of the optical absorption edge.[26,34] For C/B-codoped anatase TiO_2 (C@O&B@O) (see Fig. 4(d) and (d′)), we can see clearly that the VBM has an obvious rise of about 0.5 eV compared with that of the pure anatase TiO_2, while the conduction band bottom has a small decline of about 0.3 eV, which is mainly due to the hybridization of C 2p, B 2p and O 2p, Ti 3d states. In addition, there are many impurity states located in the band gap and a significant difference between up-spin and down-spin states for C 2p and B 2p orbitals, which may be due to spin-polarized effects and stronger interaction between the C 2p and B 2p orbitals. Therefore, the synergistic effect of C/B codoping in anatase TiO_2 can lead to a decrease of the photon excitation energy and an obvious red-shift of the optical absorption edge. The calculated result gives a good explanation for experimental optical absorption broadening to longer wavelength in C/B-codoped TiO_2. Furthermore, we calculated the Fermi level (E_F) and plotted it in Fig. 4 for anatase TiO_2. The Fermi level is pinned in the VB edge for undoped anatase TiO_2. With C doping, B doping, and C/B codoping, the Fermi level is gradually moving towards the direction of the CB edge. Our theoretical results are consistent with the previous study of Yang *et al.* for B-doped anatase TiO_2.[52] These results indicate that the TiO_2 semiconductor converts gradually from p-type characteristic to n-type characteristic with doping and codoping of impurity elements. In addition, we can clearly observe that the Fermi level crosses over the partial impurity states (see Fig. 4), especially for C doped and C/B codoped anatase TiO_2, which indicates that C doping and C/B codoping of anatase TiO_2 can make a material semi-metallic or metallic in nature.

As in the case of (co)doped rutile TiO_2, the electronic structures of all the pure and doped rutile TiO_2 models were also calculated in order to investigate the carbon and boron doping effects on the optical absorption of rutile TiO_2. The TDOS and PDOS of all the models are shown in Fig. 5, with up-spin DOS above zero and down-spin DOS below zero. For pure rutile TiO_2, the VB is mainly contributed to by the O 2p state, while the CB is mainly contributed to by the Ti 3d state, as shown in Fig. 5(a) and (a′). The calculated band gap value is 2.67 eV, which is similar to other theoretical results.[41,53] Similar to the case of C and B impurities in anatase TiO_2, C or/and B doping induces similar modifications to the electronic structures in rutile TiO_2. For C-doped rutile TiO_2 (C@O) (see Fig. 5(b) and (b′)), there are a series of down-spin impurity states (C 2p orbital) appearing in the forbidden gap, and all of the impurity energy levels are located above the VBM and below the CBM. In addition, the

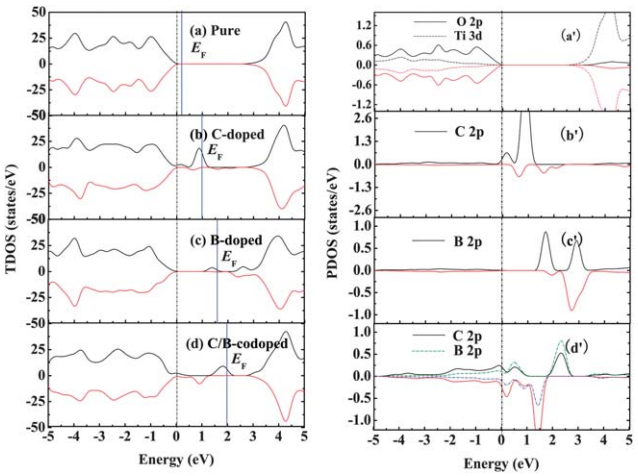

Fig. 4 The total density of states (TDOS) and partial density of states (PDOS) for the 48-atom anatase supercell ($Ti_{16}O_{32}$). (a and a′) pure, (b and b′) C-doped (C@O), (c and c′) B-doped (B@O), and (d and d′) C/B-codoped (C@O&B@O). The top of the valence band of pure anatase is taken as the reference level. The blue solid lines represent the Fermi level E_F.

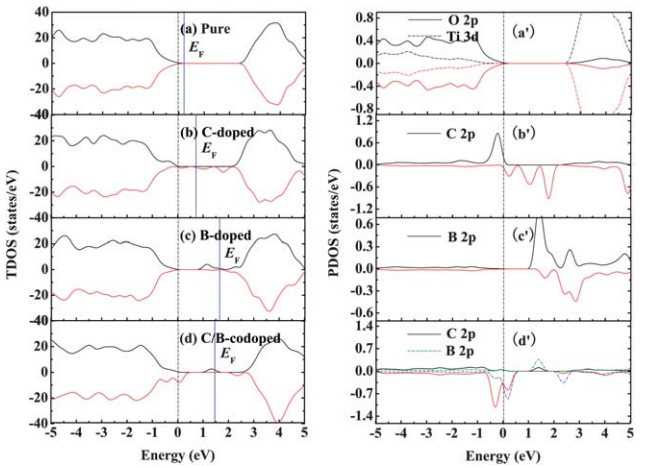

Fig. 5 The total density of states (TDOS) and partial density of states (PDOS) for the 48-atom rutile supercell ($Ti_{16}O_{32}$). (a and a′) pure, (b and b′) C-doped (C@O), (c and c′) B-doped (B@O), and (d and d′) C/B-codoped (C@O&B@O). The top of the valence band of pure rutile is taken as the reference level. The blue solid lines represent the Fermi level E_F.

CBM has an obvious decline compared with the pure rutile TiO_2, which may be due to stronger spin-polarized interactions of C 2p states. Consequently, C doping can further reduce the energy needed for electrons to be excited from VB to CB, which may be responsible for the visible-light photocatalytic activity and the red-shift phenomenon of the optical absorption edge in C-doped TiO_2. This conclusion is consistent with the experiment reported by Wu *et al.*[34] For B-doped rutile TiO_2 (B@O) (see Fig. 5(c) and (c′)), the VBM has a little shift compared with pure rutile TiO_2, and substitutional B replacing an O atom introduces some gap states bordering the CB, which are mostly composed of B 2p states and adjacent Ti 3d states. Thus, the transition energy of excited electrons from the VB to the empty states above the Fermi level may induce a red-shift of the optical absorption edge. For C/B-codoped rutile TiO_2 (C@O&B@O) (see Fig. 5(d) and (d′)), it is shown clearly that (i) the couples of the VB, C 2p and B 2p result in a broadening of the VB and a narrowing of the band gap; (ii) because of the significant difference between up-spin and down-spin states, this leads to a lot of unpaired electrons of C 2p and B 2p in the C/B-codoped rutile TiO_2 system. These unpaired electrons of C 2p and B 2p interactions lead to a series of impurity energy states (the hybridization of C 2p and B 2p orbitals) appearing in the forbidden gap. Hence, the excitation from these impurity energy states to the CB might also lead to a decrease of the photon excitation energy and induce a more significant red-shift of the absorption spectrum edge, which can possibly explain why C/B-codoped TiO_2 has better photocatalytic activity than pure TiO_2 reported in the experiment.[34] Moreover, we also calculated the Fermi level and showed it in Fig. 5 for rutile TiO_2. The Fermi level is still pinned in the VB edge for undoped rutile TiO_2. With C doping, B doping, and C/B codoping, the Fermi level is gradually moving towards the direction of the CB edge of rutile TiO_2, and also crossing over the partial impurity states (see Fig. 5). However, the Fermi level merely crosses over the edge of the partial impurity states compared with the anatase TiO_2. This result shows that C or/and B (co)doping in rutile TiO_2 can make a material appear weakly semi-metallic or metallic in nature. Therefore, TiO_2 can make a material semi-metallic or metallic in nature with C doping, B doping, and C/B codoping.

To clearly show that C or/and B doping have made a great impact on the band structure of anatase and rutile TiO_2, we plotted schematic representations of the band structures of doped anatase and rutile TiO_2 in Fig. 6 and 7, respectively. For anatase TiO_2 (see Fig. 6), the band gap is 2.90 eV without doping. (i) For the system with C doping, there is an impurity state of C 2p appearing above the VB, the energy difference between the impurity state and the CB is about 2.18 eV, and the host band gap does not change. (ii) For the system with B doping, the CB has a decline of about 0.48 eV, and the host band gap decreases to 2.42 eV. Moreover, there is an impurity state of B 2p appearing above the VB, and the energy difference between the impurity state and the VB is about 2.06 eV. (iii) For the system with C and B codoping, the VB has a rise, the CB has a decline, and the host band gap is about 2.10 eV. In addition, there are the hybridized states of C 2p and B 2p appearing in the forbidden gap. It shows the synergistic effect of carbon and

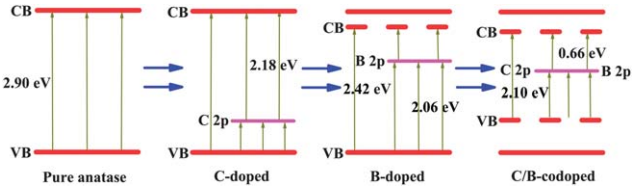

Fig. 6 Schematic representation of the band structures of pure and doped anatase TiO_2. (Energy level error is 10^{-5} eV.)

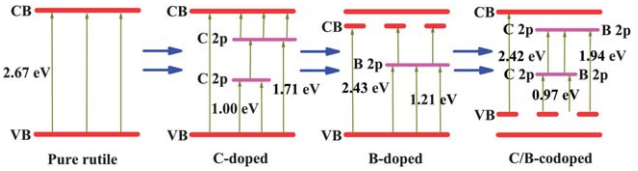

Fig. 7 Schematic representation of the band structures of pure and doped rutile TiO_2. (Energy level error is 10^{-5} eV.)

boron impurities. For rutile TiO_2 (see Fig. 7), the band gap of pure rutile is 2.67 eV. (i) For the system with C doping, the host band gap does not change. But there are two impurity states of C 2p appearing in the forbidden gap, and the energy differences between the impurity states and the VB are about 1.00 eV and 1.71 eV. (ii) For the system with B doping, the CB has a decline, and the host band gap decreases to 2.43 eV. Moreover, there is an impurity state of B 2p appearing above the VB, the energy difference between the impurity state and the VB is about 1.21 eV. (iii) For the system with C and B codoping, the VB has a rise, and the host band gap is about 2.42 eV. In addition, there are two hybridized energy states of C 2p and B 2p appearing above the VB, the energy differences between the impurity state and the VB are about 0.97 eV and 1.94 eV. It also shows the synergistic effect of carbon and boron impurities. It is well-known that the quick recombination of electron–holes is an important point in TiO_2 material. C/B codoping induces several impurity states appearing in the forbidden gap of TiO_2, these impurity states can effectively inhibit the electron transition from the CB to the VB, which reduces the recombination rate of electron–holes of TiO_2. Consequently, C/B codoping of anatase and rutile TiO_2 leads to an obvious red-shift of the absorption edge and reduces the recombination rate of electron–holes, which can result in a high photocatalytic activity of TiO_2-based materials.

Optical properties

It is well-known that optical absorption is a surface property in TiO_2. However, it is reasonable that the effect of doping on the electronic structure and optical absorption properties of anatase and rutile TiO_2 is investigated by the bulk TiO_2,[54–57] which partially reflects some experimental results. According to the obtained electronic structures, we calculated the complex dielectric function $\xi = \xi_1 + i\xi_2$.[58] The corresponding absorption spectrum was estimated by the following equation

$$I(\omega) = 2\omega\left(\frac{(\xi_1^2(\omega) + \xi_2^2(\omega))^{1/2} - \xi_1(\omega)}{2}\right)^{1/2} \quad (3)$$

where I is the optical absorption coefficient, ω is the angular frequency ($E = \hbar\omega$).

The absorption spectrum of the pure and doped TiO_2 systems are calculated and shown in Fig. 8. In anatase TiO_2 (see Fig. 8(a)), it is found that pure anatase TiO_2 can only respond to ultraviolet-light and shows no absorption response in the visible-light region. For C doped system, it exhibits a good optical absorption property in the visible-light region. Because C-doped TiO_2 has an impurity state of C 2p in the forbidden gap, it leads to a higher optical absorption performance than pure anatase TiO_2 in the long wavelength range, which is consistent with the experimental optical absorption spectrum.[34] However, it is clear that the incorporation of B into the TiO_2 lattice induces increasing optical absorption in the visible-light region, corresponding to a photo transition energy of 2.06 eV from the VB to the impurity state of B 2p. For C/B-codoped system, it is interesting that the absorption of ultraviolet- and visible-light are greatly enhanced, which is because the synergistic effect of C and B codoping can lead to a decrease of the photon excitation energy in view of the electronic structure. The results may be responsible for the outstanding photocatalytic activity and the obvious red-shift of the optical absorption edge in C/B-codoped TiO_2.

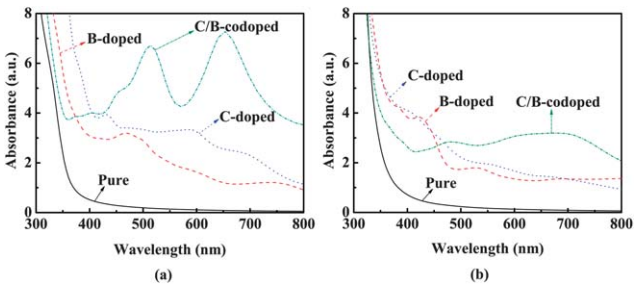

Fig. 8 The optical absorption spectra of pure and doped TiO_2 models. (a) Anatase phase and (b) rutile phase.

It is also found that the pure rutile TiO_2 (Fig. 8(b)) can only respond to ultraviolet-light and shows no absorption performance in the visible-light region. For C doped system, there are two impurity states of C 2p appearing in the band gap. Thus, the electron transition from these impurity states to the CB would lead to an obvious reduction of absorption energy and induce visible-light absorption, which also gives a good explanation for the experimental red-shift of the absorption edge.[34] For B doped system, there is an impurity state of B 2p appearing in the forbidden gap, and the CB has a decline of about 0.24 eV, which leads to a stronger absorption of visible-light. For C/B-codoped system, the VB has a rise of about 0.25 eV, and there are two hybridized states of C 2p and B 2p appearing in the band gap. Therefore, C and B codoping can further reduce the energy needed for electrons to be excited from the VB to the CB, which may be responsible for the visible-light photocatalytic activity and the red-shift phenomenon of the optical absorption edge in C/B-codoped TiO_2.

Hence, our research of the optical absorption performance of doped anatase and rutile TiO_2 indicates that the synergistic effect of C and B codoping can enhance the optical absorption of TiO_2-based materials to visible-light and induce the red-shift of the optical absorption edge, which results in an excellent photocatalytic activity in C/B-codoped TiO_2. These calculated results are consistent with the experimental reports of Wu *et al.*[34]

The influences of impurity concentration on the electronic and optical properties

To investigate the effects of impurity concentration on the electronic and optical properties for the doped anatase and rutile TiO_2 systems, we calculated the electronic structures and optical absorption spectra of different impurity concentrations in C/B-codoped anatase and rutile TiO_2. For C/B-codoped anatase TiO_2, the TDOS and absorption spectra of C/B impurity concentrations of 1.04%, 2.08% and 4.17% were calculated and are shown in Fig. 9. It is obvious that with the increase of C/B impurity concentration, the intensity of impurity states has a

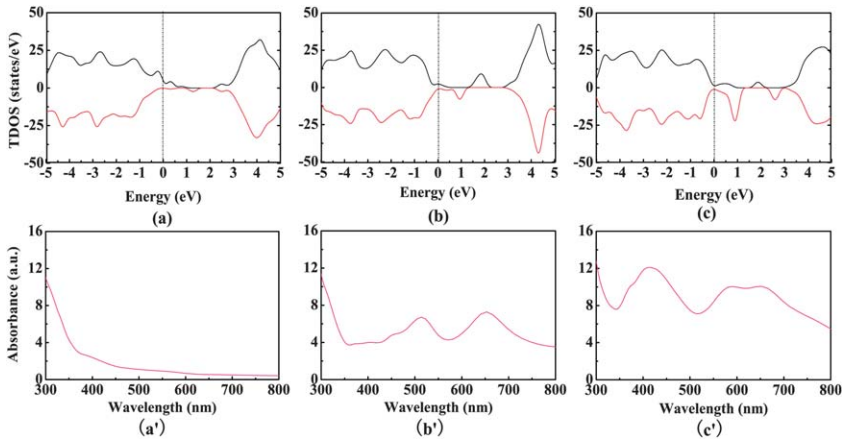

Fig. 9 The TDOS and optical absorption curves of different impurity concentrations in C/B-codoped anatase TiO_2: (a and a′) C: 1.04%, B: 1.04%; (b and b′) C: 2.08%, B: 2.08%; and (c and c′) C: 4.17%, B: 4.17%.

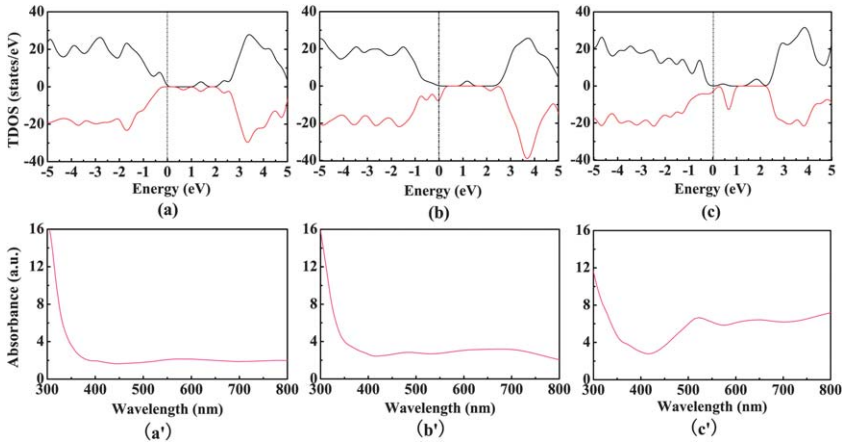

Fig. 10 The TDOS and optical absorption curves of different impurity concentrations in C/B-codoped rutile TiO_2: (a and a′) C: 1.39%, B: 1.39%; (b and b′) C: 2.08%, B: 2.08%; and (c and c′) C: 4.17%, B: 4.17%.

strengthening in the band gap and the position of impurity states changes. Moreover, the visible-light absorption performance improves gradually with the increase of C/B impurity concentration. These results are responsible for the enhanced photocatalytic activity with the increase of C/B impurity concentration. For C/B-codoped rutile TiO_2, the TDOS and absorption spectra of C/B impurity concentrations of 1.39%, 2.08% and 4.17% were also calculated, as shown in Fig. 10. With the increase of C/B impurity concentration, the variation of the impurity states and the optical absorption performance have the same trends as the C/B-codoped anatase TiO_2, which may lead to the enhanced photocatalytic activity of C/B-codoped TiO_2. Therefore, we obtain the same conclusions for the codoped anatase and rutile phase TiO_2 systems. The conclusions are consistent with the experimental results of Wu *et al.*[34]

4 Conclusions

We have studied the electronic and optical properties of several possible C-doped, B-doped, and C/B-codoped models of anatase and rutile TiO_2 systematically using spin-polarized DFT calculations based on the plane-wave method. The calculated results show that (i) C/B codoping of anatase TiO_2 can induce some hybridized energy states (C 2p and B 2p) appearing in the forbidden gap and the band gap has a narrowing by about 0.8 eV, which leads to a red-shift phenomenon of the optical absorption edge in TiO_2; (ii) the couples of the VB, C 2p and B 2p result in a broadening of the VB and a narrowing of the band gap in C/B-codoped rutile TiO_2, which can also induce a red-shift of the optical absorption edge. Therefore, the synergistic effect of C/B codoping in anatase and rutile TiO_2 can lead to a decrease of the photon excitation energy and an obvious red-shift of the optical absorption edge. In addition, we have also investigated the influences of impurity concentration on the electronic and optical properties. The investigated results indicate that the intensity of impurity states has a strengthening in the band gap, the position of impurity states changes, and the visible-light absorption performance improves gradually with the increase of C/B impurity concentration in C/B-codoped anatase and rutile TiO_2. In summary, the synergistic effect of C and B codoping can enhance the optical absorption of TiO_2 in the visible-light region and induce the red-shift of the optical absorption edge, which results in an excellent photocatalytic activity in C/B-codoped TiO_2.

Acknowledgements

Yanming Lin would like to thank Dr Kesong Yang and Dr Run Long for helpful discussions. This work was supported by the National Science Foundation of China under Grants (no.s 10647008, 50971099, and 21176199), the Research Fund for the Doctoral Program of Higher Education (no.s 20096101110017 and 20096101110013), Key Project of Natural Science Foundation of Shaanxi Province of China (no.s 2010JZ002 and 2011JM1001), and Graduate's Innovation Fund of Northwest University of China (no. YZZ12082).

Notes and references

1 S. Y. Huang, L. Kavan, I. Exnar and M. Grätzel, *J. Electrochem. Soc.*, 1995, **142**, L142.
2 S. U. M. Khan, M. Al-Shahry and W. B. Ingler, *Science*, 2002, **297**, 2243.
3 A. Fujishima and K. Honda, *Nature*, 1972, **238**, 37.
4 M. R. Hoffmann, S. T. Martin, W. W. Choi and D. W. Bahnemann, *Chem. Rev.*, 1995, **95**, 69.
5 Y. Lin, Z. Jiang, C. Zhu, X. Hu, X. Zhang, H. Zhu and J. Fan, *Appl. Phys. Lett.*, 2012, **101**, 062106.
6 W. J. Yin, H. Tang, S. H. Wei, M. M. Al-Jassim, J. Turner and Y. Yan, *Phys. Rev. B: Condens. Matter Mater. Phys.*, 2010, **82**, 045106.
7 H. Tang, F. Lévy, H. Berger and P. E. Schmid, *Phys. Rev. B: Condens. Matter*, 1995, **52**, 7771.
8 F. Arntz and Y. Yacoby, *Phys. Rev. Lett.*, 1966, **17**, 857.
9 Y. Gai, J. Li, S. S. Li, J. B. Xia and S. H. Wei, *Phys. Rev. Lett.*, 2009, **102**, 036402.
10 R. Jin, Z. Wu, Y. Liu, B. Jiang and H. Wang, *J. Hazard. Mater.*, 2009, **161**, 42.

11 K. Yang, Y. Dai and B. Huang, *Chem. Phys. Lett.*, 2008, **456**, 71.
12 R. Asahi, T. Morikawa, T. Ohwaki, K. Aoki and Y. Taga, *Science*, 2001, **293**, 269.
13 H. Irie, Y. Watanabe and K. Hashimoto, *J. Phys. Chem. B*, 2003, **107**, 5483.
14 T. Lindgren, J. M. Mwabora, E. Avendaño, J. Jonsson, A. Hoel, C. G. Granqvist and S. E. Lindquist, *J. Phys. Chem. B*, 2003, **107**, 5709.
15 C. DiValentin, G. Pacchioni and A. Selloni, *Phys. Rev. B: Condens. Matter Mater. Phys.*, 2004, **70**, 085116.
16 L. Jung-Yup, P. Jaewon and C. Jun-Hyung, *Appl. Phys. Lett.*, 2005, **87**, 011904.
17 K. Yang, Y. Dai, B. Huang and S. Han, *J. Phys. Chem. B*, 2006, **110**, 24011.
18 M. Batzill, E. H. Morales and U. Diebold, *Phys. Rev. Lett.*, 2006, **96**, 026103.
19 T. Umebayashi, T. Yamaki, H. Itoh and K. Asai, *Appl. Phys. Lett.*, 2002, **81**, 454.
20 T. Umebayashi, T. Yamaki, S. Yamamoto, A. Miyashita and S. Tanaka, *J. Appl. Phys.*, 2003, **93**, 5156.
21 J. C. Yu, W. Ho, J. Yu, H. Yip, P. K. Wong and J. Zhao, *Environ. Sci. Technol.*, 2005, **39**, 1175.
22 F. Tian and C. Liu, *J. Phys. Chem. B*, 2006, **110**, 17866.
23 C. D. Valentin, G. Pacchioni and A. Selloni, *Chem. Mater.*, 2005, **17**, 6656.
24 H. Wang and J. P. Lewis, *J. Phys.: Condens. Matter*, 2005, **17**, L209.
25 F. Dong, S. Guo, H. Wang, X. Li and Z. Wu, *J. Phys. Chem. C*, 2011, **115**, 13285.
26 W. Zhao, W. Ma, C. Chen, J. Zhao and Z. Shuai, *J. Am. Chem. Soc.*, 2004, **126**, 4782.
27 C. -H. Wei, X. -H. Tang, J. -R. Liang and S. -Y. Tan, *J. Environ. Sci.*, 2007, **19**, 90.
28 M. Bettinelli, V. Dallacasa, D. Falcomer, P. Fornasiero, V. Gombac, T. Montini, L. Romanó and A. Speghini, *J. Hazard. Mater.*, 2007, **146**, 529.
29 D. Chen, D. Yang, Q. Wang and Z. Jiang, *Ind. Eng. Chem. Res.*, 2006, **45**, 4110.
30 K. Y. Jung, S. B. Park and S. -K. Ihm, *Appl. Catal., B*, 2004, **51**, 239.
31 L. Jia, C. Wu, Y. Li, S. Han, Z. Li, B. Chi, J. Pu and L. Jian, *Appl. Phys. Lett.*, 2011, **98**, 211903.
32 N. Li, K. L. Yao, L. Li, Z. Y. Sun, G. Y. Gao and L. Zhu, *J. Appl. Phys.*, 2011, **110**, 073513.
33 R. Long and N. J. English, *New J. Phys.*, 2012, **14**, 053007.
34 Y. Wu, M. Xing and J. Zhang, *J. Hazard. Mater.*, 2011, **192**, 368.
35 G. Kresse and J. Hafner, *Phys. Rev. B: Condens. Matter*, 1994, **49**, 14251.
36 G. Kresse and J. Furthmüller, *Phys. Rev. B: Condens. Matter*, 1996, **54**, 11169.
37 J. P. Perdew, C. J. Ahevary, S. H. Vosko, K. A. Jackson, M. R. Pederson, D. J. Singh and C. Fiolhais, *Phys. Rev. B: Condens. Matter*, 1992, **46**, 6671.
38 H. J. Monkhorst and J. D. Pack, *Phys. Rev. B: Solid State*, 1976, **13**, 5188.
39 S. L. Dudarev, G. A. Botton, S. Y. Savarsov, C. J. Humphreys and A. P. Sutton, *Phys. Rev. B: Condens. Matter Mater. Phys.*, 1998, **57**, 1505.
40 K. Yang, Y. Dai, B. Huang and Y. P. Feng, *Phys. Rev. B: Condens. Matter Mater. Phys.*, 2010, **81**, 033202.
41 K. Yang, Y. Dai, B. Huang and M. H. Whangbo, *J. Phys. Chem. C*, 2009, **113**, 2624.
42 M. E. Arroyo-de Dompablo, A. Morales-García and M. Taravillo, *J. Chem. Phys.*, 2011, **135**, 054503.
43 J. K. Burdett, T. Hughbanks, G. J. Miller, J. W. Richardson, J. V. Smith Jr and J. V. Smith, *J. Am. Chem. Soc.*, 1987, **109**, 3639.
44 C. DiValentin, G. Pacchioni and A. Selloni, *Phys. Rev. B: Condens. Matter Mater. Phys.*, 2004, **70**, 085116.
45 H. Weng, J. Dong, T. Fukumura, M. Kawasaki and Y. Kawazoe, *Phys. Rev. B: Condens. Matter Mater. Phys.*, 2006, **73**, 121201(R).
46 R. Janisch and N. A. Spaldin, *Phys. Rev. B: Condens. Matter Mater. Phys.*, 2006, **73**, 035201.
47 H. Tang, H. Berger, P. E. Schmid, F. Lévy and G. Burri, *Solid State Commun.*, 1993, **87**, 847.
48 J. Pascual, J. Camassel and H. Mathieu, *Phys. Rev. Lett.*, 1977, **39**, 1490.
49 J. Pascual, J. Camassel and H. Mathieu, *Phys. Rev. B*, 1978, **18**, 5606.
50 R. S. Mulliken, *J. Chem. Phys.*, 1955, **23**, 1833.
51 I. G. Csizmadia, *Theory and Practice of MO Calculations on Organic Molecules*, Elsevier, Amsterdam, 1976.
52 K. Yang, Y. Dai and B. Huang, *J. Phys. Chem. C*, 2010, **114**, 19830.
53 Y. M. Lin, Z. Y. Jiang, C. Y. Zhu, X. Y. Hu, X. D. Zhang and J. Fan, *Mater. Chem. Phys.*, 2012, **133**, 746.
54 K. Yang, Y. Dai and B. Huang, *J. Phys. Chem. C*, 2007, **111**, 12086.
55 R. Shirley, M. Kraft and O. R. Inderwildi, *Phys. Rev. B: Condens. Matter Mater. Phys.*, 2010, **81**, 075111.
56 L. Jia, C. Wu, S. Han, N. Yao, Y. Li, Z. Li, B. Chi, J. Pu and L. Jian, *J. Alloys Compd.*, 2011, **509**, 6067.
57 Y. Lin, Z. Jiang, X. Hu, X. Zhang and J. Fan, *Appl. Phys. Lett.*, 2012, **100**, 102105.
58 B. Adolph, J. Furthmüller and F. Bechstedt, *Phys. Rev. B: Condens. Matter*, 2001, **63**, 125108.

